ACS OMEGA

http://pubs.acs.org/journal/acsodf

Article

# Structural Conformation and Activity of Spider-Derived Inhibitory Cystine Knot Peptide Pn3a Are Modulated by pH

Poanna Tran, Theo Crawford, Lotten Ragnarsson, Jennifer R. Deuis, Mehdi Mobli, Simon J. Sharpe, Christina I. Schroeder,* and Irina Vetter*

Cite This: *ACS Omega* 2023, 8, 26276−26286

Read Online

ACCESS | Metrics & More | Article Recommendations | Supporting Information

**ABSTRACT:** Numerous spider venom-derived gating modifier toxins exhibit conformational heterogeneity during purification by reversed-phase high-performance liquid chromatography (RP-HPLC). This conformational exchange is especially peculiar for peptides containing an inhibitor cystine knot motif, which confers excellent structural stability under conditions that are not conducive to disulfide shuffling. This phenomenon is often attributed to proline *cis*/*trans* isomerization but has also been observed in peptides that do not contain a proline residue. Pn3a is one such peptide forming two chromatographically distinguishable peaks that readily interconvert following the purification of either conformer. The nature of this exchange was previously uncharacterized due to the fast rate of conversion in solution, making isolation of the conformers impossible. In the present study, an N-terminal modification of Pn3a enabled the isolation of the individual conformers, allowing activity assays to be conducted on the individual conformers using electrophysiology. The conformers were analyzed separately by nuclear magnetic resonance spectroscopy (NMR) to study their structural differences. RP-HPLC and NMR were used to study the mechanism of exchange. The later-eluting conformer was the active conformer with a rigid structure that corresponds to the published structure of Pn3a, while NMR analysis revealed the earlier-eluting conformer to be inactive and disordered. The exchange was found to be pH-dependent, arising in acidic solutions, possibly due to reversible disruption and formation of intramolecular salt bridges. This study reveals the nature of non-proline conformational exchange observed in Pn3a and possibly other disulfide-rich peptides, highlighting that the structure and activity of some disulfide-stabilized peptides can be dramatically susceptible to disruption.

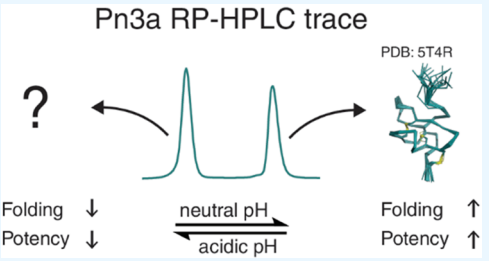


## INTRODUCTION

Animal venoms are a rich source of potential therapeutic peptides with high selectivity, potency, and stability.[1−3] Neuronal ion channels are a common target for venom peptides, including voltage-gated sodium channels ($Na_V$s) involved in pain signal transduction.[1−4] The $Na_V$ subtype 1.7 ($Na_V1.7$) is believed to be an attractive target for the treatment of pain because this subtype is expressed preferentially in peripheral sensory neurons,[4,5] and its crucial role in pain sensation has been genetically validated.[6−8] Selectivity for $Na_V1.7$ remains a challenge due to the high sequence similarity across all $Na_V$ subtypes, but it is vital for reducing unwanted and dangerous side effects.[4]

Pn3a is a potent $Na_V1.7$-inhibiting peptide derived from the venom of the tarantula *Pamphobeteus nigricolor*.[9] It is highly selective for $Na_V1.7$ over all other $Na_V$ subtypes,[9] and Pn3a variants with improved potency and selectivity have been designed, including [D8N]Pn3a,[10] which was used in this study. Pn3a binds to the voltage sensor domains II and IV (VSDII, VSDIV) of $Na_V1.7$, affecting the voltage dependence of activation and fast inactivation of the channel.[9] Like many other venom-derived peptides, the structure of Pn3a is stabilized by three disulfide bonds arranged in an inhibitor cystine knot (ICK) which confers excellent stability under a wide range of conditions (Figure 1A).[9,11,12]

Interestingly, Pn3a is known to form two peaks of roughly equal proportion by reversed-phase high-performance liquid chromatography (RP-HPLC) during purification, despite its disulfide connectivity remaining intact.[10,13] Separation of the two peaks by RP-HPLC fails to isolate a single conformer because the peptide exchanges quickly in solution, regenerating the two conformers in roughly equal proportions.[13] This phenomenon has been observed in other spider venom-derived peptides with similar sequences, although RP-HPLC traces typically show a major and minor species rather than two equally populated peaks.[14−16] However, these conformers have yet to be isolated or characterized successfully due to their rapid return to equilibrium in HPLC solvents. Nuclear magnetic resonance spectroscopy (NMR) experiments have

Received: April 18, 2023
Accepted: June 22, 2023
Published: July 11, 2023

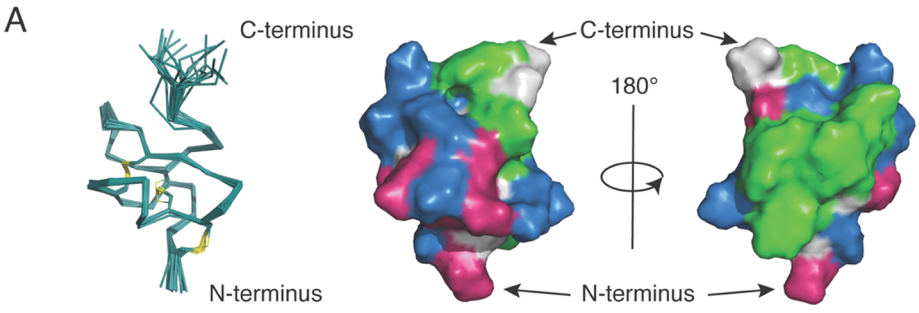


B

| Peptide | Sequence | % Similarity |
|---|---|---|
| | Loop 1 2 3 4 | |
| [D8N]Pn3a[9, 10] | -----DCRYMFGNCEKDEDCCKHLGCKRKMK--YCAWDFTFT | 100 |
| HaTx1[28] | -----ECRYLFGGCKTTSDCCKHLGCKFRDK--YCAWDFTFS | 68.6 |
| HaTx2[28] | -----ECRYLFGGCKTTADCCKHLGCKFRDK--YCAWDFTFS | 68.6 |
| Mb1a[26] | GVDKPGCRYMFGGCVQDDDCCPHLGCKRKGL--YCAWDGT | 63.2 |
| Hm1b[30] | -----ECRYLFGGCKTTADCCKHLGCRTDLY--YCAWDGTF* | 61.8 |
| PcaTX-1[27] | ----AGCKYLFGSCKEDSDCCKHLGCRRKAPQ-YCGWDGTF | 61.1 |
| Eo1a[29] | -----DCRWFLGGCSKDSDCCKHLACRIDGYIKYCAWDGTF | 61.1 |
| Mb1b[26] | GVDKPGCRYMFGGCVQDDDCCPHLGCKRKGL--YCAWDAS | 60.5 |
| Hm1a[30] | -----ECRYLFGGCSSTSDCCKHLSCRSDWK--YCAWDGTFS | 60.0 |
| Cc1a[15] | GVDKEGCKYMFGSCGKSDDCCPKLACKRTFN--YCAWDGSV | 48.7 |
| Df1a[14] | -----ECRWFLGGCSGGQTCCEHLVCHRKHQ--WCVWDWSF | 44.1 |
| SGTx1[36] | -----TCRYLFGGCKTTADCCKHLACRSDGK--YCAWDGTF | 63.6 |
| ProTx-II[37] | -----YCQKWMWTCDSERKCCEGMVCRL-----WCKKKLW | 20.0 |
| Colour code: | Acidic Basic Hydrophobic Cysteine Proline | |

**Figure 1.** Solution NMR structure of Pn3a and sequences of similar spider venom-derived peptides. (A) Ribbon and surface structures of Pn3a (PDB 5T4R) showing acidic (pink), basic (blue), and aromatic/hydrophobic (green) residues. Disulfide bonds are shown in yellow. (B) Sequence of [D8N]Pn3a with disulfide connectivity shown above, aligned with sequences of similar spider venom-derived peptides that exhibit conformational exchange by RP-HPLC. The sequences of SGTx1 and ProTx-II, which do not exhibit conformational heterogeneity, are also shown. Percent similarity to [D8N]Pn3a is shown. *Indicates amide C-terminus.

been used to elucidate the three-dimensional structure of Pn3a in water at pH 4,[9] but these spectra show only one set of peaks, indicative of a single folded state.[9,13]

Proline *cis/trans* isomerization has been shown to be responsible for structural heterogeneity in other venom peptides,[17−19] and can act as a "switch" causing conformational changes in proteins, which are crucial for function.[20−24] μ-Aga-I and μ-Aga-IV are spider venom-derived peptides that each form two proline *cis/trans* conformers.[17] The *cis* isomer dominates in μ-Aga-I, while both the *cis* and *trans* isomers are found in equal proportions in μ-Aga-IV.[17] Despite having high sequence similarity, these two peptides differ in the site of proline isomerization.[17] ACTX-Hi:OB4219 is another spider venom-derived peptide that also exists in two equally proportioned proline *cis/trans* isomers, which can be distinguished by NMR but not by RP-HPLC.[18] Several other spider venom peptides that are conformationally heterogeneous by RP-HPLC are assumed to undergo *cis/trans* proline isomerization if they contain at least one proline residue.[15,25,26]

Pn3a and some other exchanging peptides with similar sequences do not contain a proline residue (Figure 1B),[9,14,27−30] so their conformational heterogeneity must be due to some other type of conformational exchange. HaTx1, HaTx2, Hm1a, Hm1b, Eo1a, and Df1a are additional examples of peptides behaving in a similar manner.[14,28−30] Because these peptides, and others that share similar sequences to Pn3a, are ion channel modulators, they can be used to study and characterize ion channels in vitro, and some may have the potential for development as therapeutics. Therefore, it is important to identify any differences in the structure and activity between the conformers and to understand the conditions that give rise to this exchange. The heterogeneity of HaTx1 and HaTx2 was hypothesized to be due to disulfide bond rotational isomerization,[31] which has also been described in the polypeptide BPTI.[32] Rotational isomerization of aromatic side chains about their Cβ−Cγ bonds has also been described in BPTI.[33] The spider venom peptide PcaTX-1 forms two peaks by RP-HPLC due to aspartate to isoaspartate conversion facilitated by the presence of a subsequent glycine residue.[27] The spider venom peptide Pre1a also elutes in multiple peaks by RP-HPLC.[34] Although it contains two proline residues, its conformational flexibility was shown by NMR to originate from the movement of a single flexible loop, possibly due to the overcrowding of bulky aromatic side chains, which does not seem to involve proline isomerization.[34]

In this study, [D8N]Pn3a, which exhibits the same conformational heterogeneity as the native Pn3a, was N- or C-terminally ligated to an inactive analogue of KIIIA (a $Na_V$-inhibiting cone snail venom peptide)[35] via copper-mediated azide-alkyne cycloaddition (CuAAC) or sortase A-mediated enzymatic ligation, respectively. N-terminal ligation resulted in a decreased rate of conformational exchange in a solution that enabled the isolation of each conformer. The activity and structure of these peptides were studied using patch-clamp


https://doi.org/10.1021/acsomega.3c02664
ACS Omega 2023, 8, 26276−26286

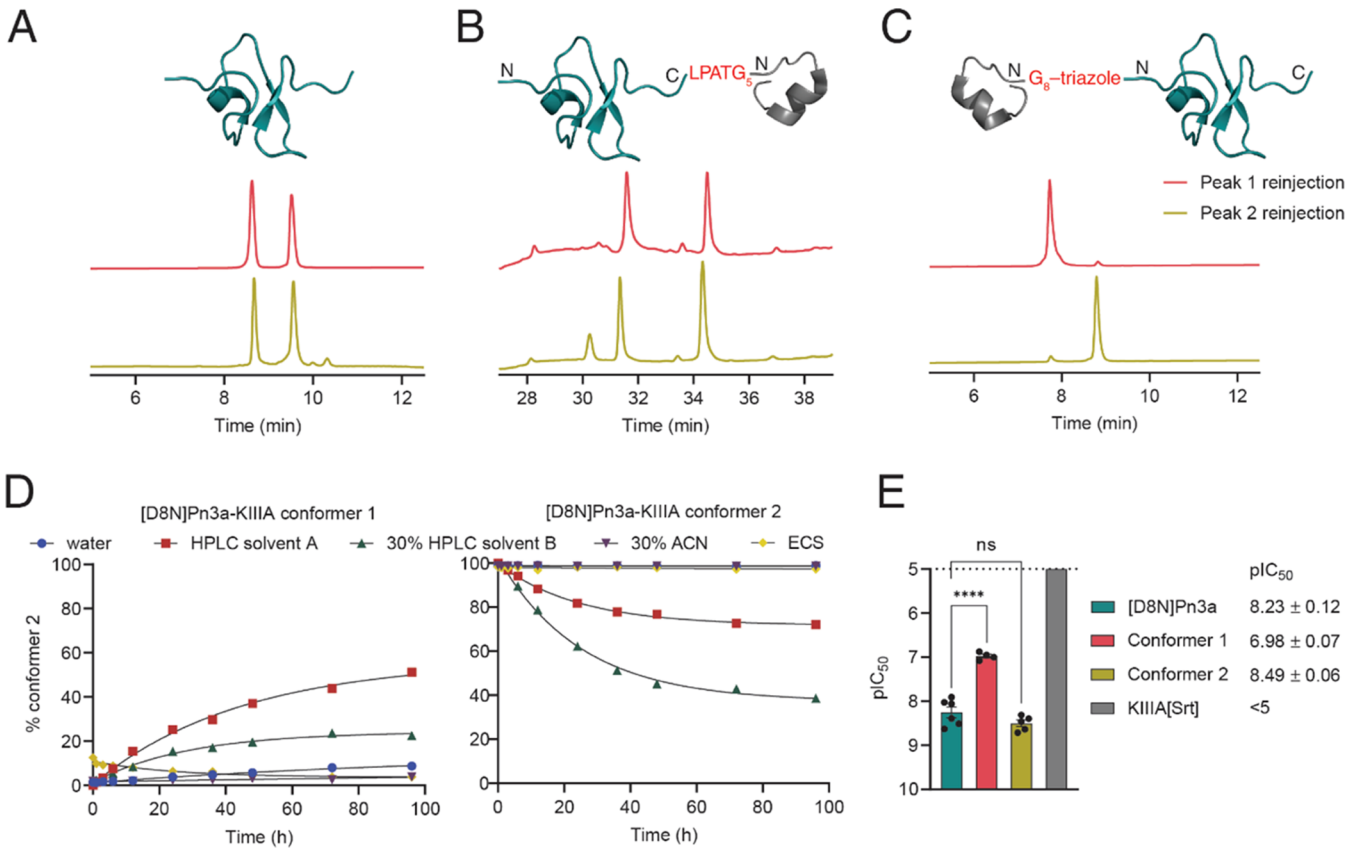


**Figure 2.** Ligated [D8N]Pn3a-KIIIA exhibits slower exchange than the monovalent peptide, enabling the isolation of each conformer. The early-eluting conformer 1 of Pn3a is less potent than the later-eluting conformer 2. RP-HPLC elution profiles within 6 h of collection of each peak of (A) [D8N]Pn3a, (B) C−N-ligated [D8N]Pn3a-KIIIA, and (C) N−N-ligated [D8N]Pn3a-KIIIA. Pn3a is shown in teal (PDB 5T4R) with N- and C-termini indicated, and KIIIA is shown in gray (PDB 2LXG). Linkers are shown in red. (D) Stability time course over 96 h of [D8N]Pn3a-KIIIA in varying solvent conditions starting with >95% conformer 1 (left) or conformer 2 (right). (E) $pIC_{50}$ ($-\log IC_{50}$) values of [D8N]Pn3a, [D8N]Pn3a-KIIIA[Srt] conformer 1 and conformer 2, and KIIIA[Srt] at $hNa_V1.7$. *$p < 0.05$ by one-way ANOVA with Dunnett's multiple comparisons test compared to [D8N]Pn3a. Data are presented as the mean ± SEM ($n$ = 4−6 cells).

electrophysiology and NMR spectroscopy, highlighting how easily the structure and activity of some ICK-stabilized peptides can be disrupted and restored.

## RESULTS

**N-Terminal Modification of Pn3a Slows Conformational Exchange.** As previously reported,[10,13] the RP-HPLC trace of correctly folded Pn3a contains two peaks that are regenerated when a single peak is collected and reinjected (Figures 2A and S1A). A similar result was obtained for all Pn3a analogues comprising native disulfide connectivity of Pn3a.[10] Bivalent analogues of [D8N]Pn3a containing μ-conotoxin KIIIA attached at either the C- or N-terminus were synthesized for a previous study to create $Na_V1.7$ inhibitors with dual modes of action (Table S1). Surprisingly, while the C-terminally modified bivalent peptide regenerated its two peaks (Figure 2B), the N-terminally modified peptide did not exhibit the same peak regeneration under the same conditions (Figures 2C and S1B), suggesting slower exchange between the two conformers. This allowed for each conformer of N−N-ligated [D8N]Pn3a-KIIIA to be isolated with >95% purity by HPLC.

**Stability of [D8N]Pn3a-KIIIA Conformers.** The stability of each N−N-ligated [D8N]Pn3a-KIIIA conformer in various solvents was determined by HPLC. Each of the conformers was maintained over at least 96 h in unbuffered milliQ water as well as extracellular solution (ECS) buffer for electrophysiology experiments (70 mM NaCl, 70 mM choline chloride, 4 mM KCl, 2 mM $CaCl_2$, 1 mM $MgCl_2$, 10 mM HEPES, and 10 mM glucose, adjusted to pH 7.4 and 305 mOsm), suggesting that these conditions would be suitable for NMR experiments and activity assays, respectively (Figure 2D). The stability of the conformers was also evaluated over 96 hours in HPLC solvents (Figure 2D). Both conformers exchanged in 30% HPLC solvent B (0.05% TFA/30% ACN/$H_2O$), the acetonitrile concentration at which the peptide elutes, approaching an equilibrium favouring the earlier-eluting conformer (conformer 1). In HPLC solvent A (0.05% TFA/$H_2O$), the conformers approached an equilibrium favouring the later-eluting conformer (conformer 2). The same time-course experiment was performed in 30% ACN/$H_2O$, which did not cause conformational exchange after 96 h, suggesting that acidification by TFA caused the exchange to occur.

**Activity of Individual Conformers of Pn3a.** In light of the excellent stability of either conformer in an aqueous solution, we next assessed the activity of each conformer at $hNa_V1.7$ to determine whether they differed in potency (Figure 2E). We used [D8N]Pn3a ligated to a KIIIA analogue inactivated by the sortase A ligation motif LPATGG in the C-terminus (KIIIA[Srt])[35] to assess only activity arising from [D8N]Pn3a (Table S1). The ligated peptide, [D8N]Pn3a-KIIIA[Srt], exhibited a similar slow rate of exchange to the


https://doi.org/10.1021/acsomega.3c02664
ACS Omega 2023, 8, 26276−26286

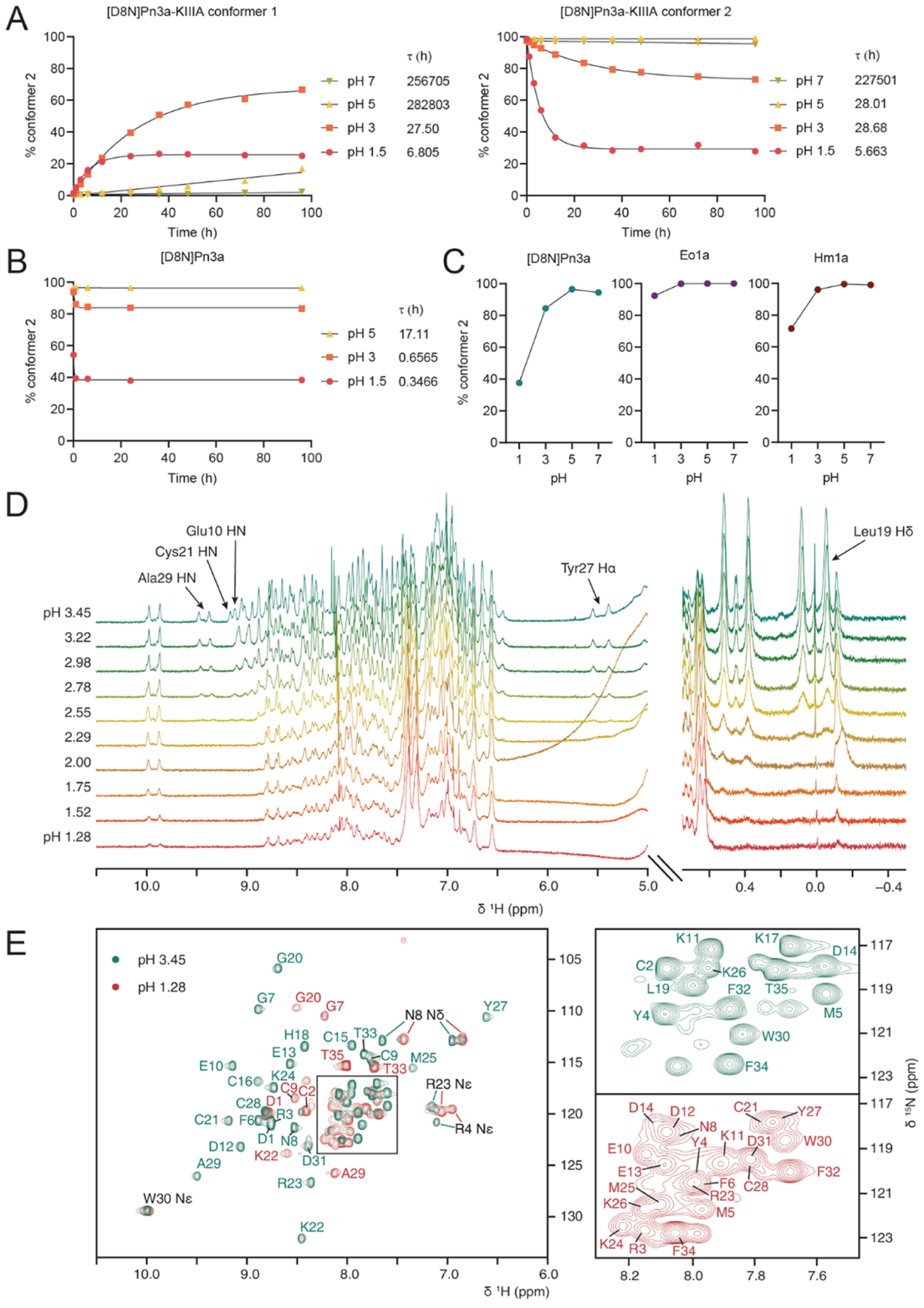


**Figure 3.** Conformational exchange of Pn3a is pH-dependent, favouring the more active conformer 2 at higher pH values. Percentages are calculated from the area under the curve of RP-HPLC traces. (A) Exchange time course of [D8N]Pn3a-KIIIA at varying pH by RP-HPLC starting with >95% conformer 1 (left) or conformer 2 (right). (B) Exchange time course of [D8N]Pn3a at varying pH by RP-HPLC. (C) Later-eluting conformer percentages of [D8N]Pn3a, Eo1a, and Hm1a at equilibrium after >1 h incubation at varying pH by RP-HPLC. (D) Stacked 1D $^{1}$H NMR amide region and far upfield aliphatic region of $^{13}$C/$^{15}$N-[S0,D8N]Pn3a as pH was increased from 1.28 to 3.45. (E) Overlaid 2D $^{1}$H−$^{15}$N HSQC assignments of $^{13}$C/$^{15}$N-[S0,D8N]Pn3a at pH 1.28 and 3.45. The inset square denotes the expanded and separated areas of spectra shown for clarity (right).

peptide containing wildtype KIIIA (Figure S2). The individual [D8N]Pn3a and KIIIA[Srt] peptides displayed the expected potencies at hNa$_V$1.7 (pIC$_{50}$ 8.23 ± 0.12 and inactive up to 10 $\mu$M, respectively) (Figure 2E).[10,35] The [D8N]Pn3a-KIIIA-



https://doi.org/10.1021/acsomega.3c02664
ACS Omega 2023, 8, 26276−26286

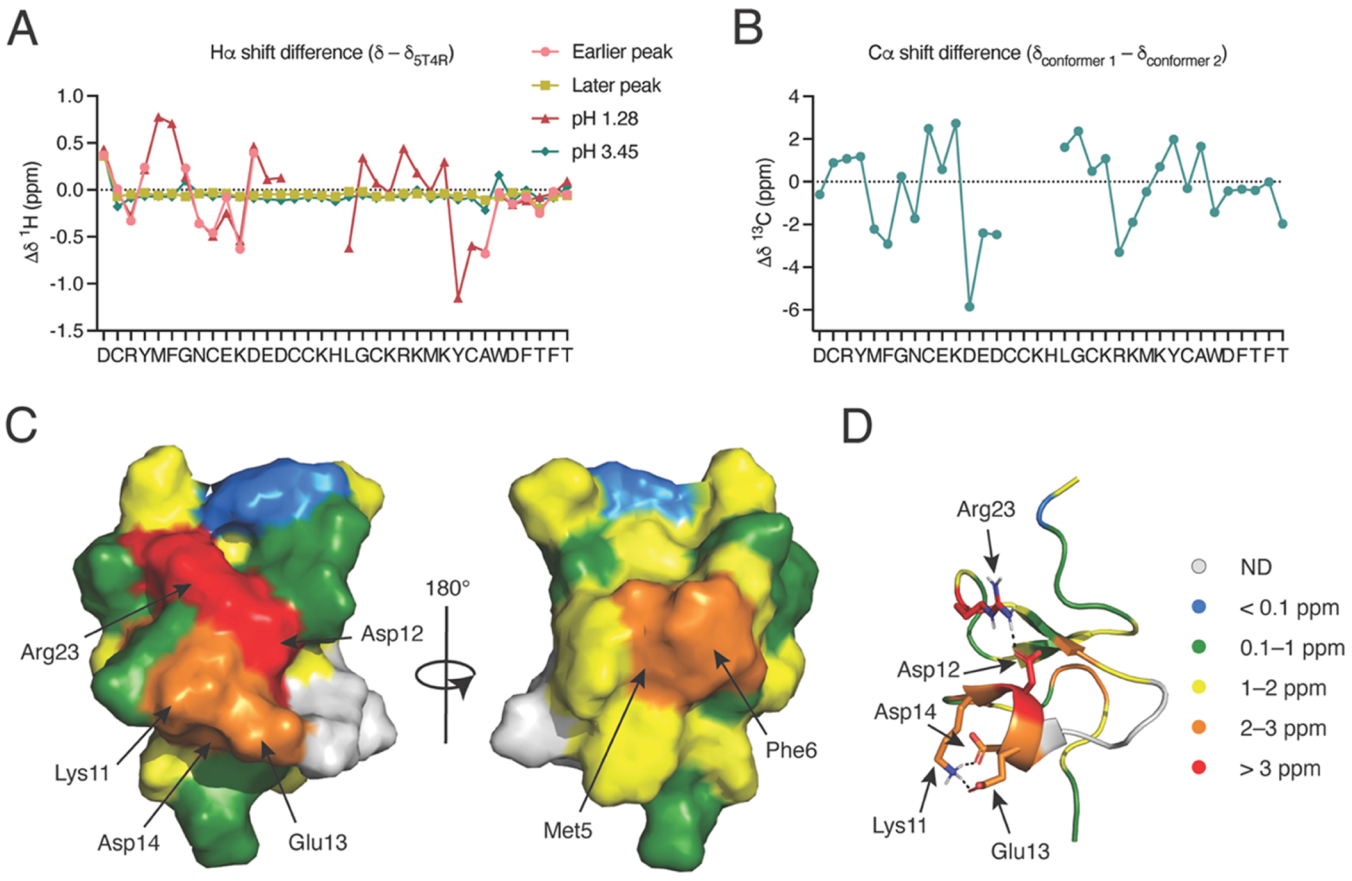


**Figure 4.** Conformer 2 corresponds to the published Pn3a structure. Conformer 1 differs drastically from conformer 2. (A) Difference in Pn3a H$\alpha$ shifts of earlier- and later-eluting [D8N]Pn3a-KIIIA conformers from 2D $^{1}$H−$^{1}$H TOCSY and NOESY experiments, and pH 1.28 and 3.45 $^{13}$C/$^{15}$N-[S0,D8N]Pn3a conformers from 3D $^{1}$H−$^{15}$N−$^{13}$C CBCA(CO)NH and HNCACB experiments, compared to published shifts for Pn3a (PDB 5T4R). (B) Difference in C$\alpha$ shifts of $^{13}$C/$^{15}$N-[S0,D8N]Pn3a conformer 1 compared to conformer 2. (C) Surface structure heat map of Pn3a (conformer 2), indicating the magnitudes of C$\alpha$ shift differences. Residues with $\Delta\delta > 2$ are labeled. (D) Cartoon structure of Pn3a (PDB 5T4R) with putative side-chain salt bridges between residues with $\Delta\delta > 2$ shown by dashed lines.

[Srt] conformer 1 was 32-fold less potent than conformer 2 ($pIC_{50}$ 6.98 ± 0.07 and 8.49 ± 0.06, respectively, $p < 0.05$) (Figure 2E).

**pH-Dependence of Exchange by RP-HPLC.** To confirm a possible contribution of pH to the conformational exchange, an HPLC time course was performed using [D8N]Pn3a-KIIIA in solutions at pH 1 (100 mM HCl), pH 3 (20 mM potassium phosphate), pH 5 (20 mM sodium citrate), and pH 7 (20 mM potassium phosphate) (Figure 3A). The conformers reached equilibrium within 24 h at pH 1, favouring conformer 1. At pH 3, the conformers did not reach equilibrium after 96 h but favored conformer 2. At pH 5, conformer 1 began to exchange but did not reach equilibrium after 96 h, while conformer 2 did not appear to exchange. Both conformers were stable at pH 7 over at least 96 h. These results suggest that both the rate of exchange and the proportion of each conformer at equilibrium are pH-dependent.

The same experiment was then performed using monovalent [D8N]Pn3a (Figures 3B and S3A). In all pH-adjusted solutions, the peptide exchanged between conformers quickly, reaching equilibrium within 1 h. A similar pattern of pH-dependence was observed compared to the ligated peptide, with conformer 1 arising at pH < 5 and the proportion of conformer 1 increasing as pH decreased. Although a higher ion concentration was required to attain pH 1, the exchange was not dependent on ion concentration as no exchange was observed in a buffer at pH 7 containing 100 mM NaCl (Figure S3A). The pH-dependence of exchange was also evaluated for Eo1a and Hm1a, which are proline-free peptides showing conformational heterogeneity by RP-HPLC.[29,30] Lower pH gave rise to an earlier-eluting peak in the elution profiles of these peptides, although the relative proportion of this conformer never exceeded that of the later-eluting conformer at the lowest tested pH (Figures 3C and S3B,C). To assess whether a similar pH-dependent exchange can also occur for other proline-free $Na_V1.7$ inhibitors, ProTx-II and SGTx1, which each elute in a single peak, were similarly evaluated.[36,37] Both of these peptides showed no exchange at low pH or high ion concentration (Figure S3D,E), suggesting that exchange for Pn3a and related peptides is likely sequence-specific rather than a general feature of disulfide-rich ICK peptides.[11,12]

**pH-Dependence of Exchange by NMR.** The $^{13}$C/$^{15}$N-labeled analogue [S0,D8N]Pn3a was produced by the recombinant expression for use in NMR experiments, with an N-terminal serine scar remaining after TEV cleavage from SUMO.[13] 1D $^{1}$H− and 2D $^{1}$H−$^{15}$N HSQC were acquired as pH was increased incrementally from pH 1.28−3.45. The amide regions of the 1D spectra revealed less dispersed (<9 ppm) and broader peaks at low pH, suggesting the peptide was disordered (Figure 3D). As pH increased, the amide region became populated with sharper peaks which also appeared downfield of 9 ppm, consistent with previously published 1D


https://doi.org/10.1021/acsomega.3c02664
ACS Omega 2023, 8, 26276−26286

spectra for Pn3a.[9,10,13] Similarly, $^{1}H-^{15}N$ HSQC data showed resonances corresponding to the published Pn3a shifts appearing as the sample pH increased, indicating a transition from conformer 1 to conformer 2 (Figure 3E).

**Structural Comparison of Conformers.** 2D $^{1}H-^{1}H$ TOCSY and NOESY NMR experiments were used to characterize the structures of conformers 1 and 2 of [D8N]Pn3a-KIIIA. All KIIIA backbone chemical shifts were consistent between both conformers, whereas [D8N]Pn3a spectra differed considerably (Figure S4). All [D8N]Pn3a backbone protons were successfully assigned for conformer 2, which produced high-quality spectra (Figure S4B). Only a partial backbone assignment was completed for conformer 1 using these spectra, which produced fewer peaks than expected, and many peaks of low intensity (Figure S4A). Due to the reduced dispersion of the amide protons, the spectra also contained regions of significant overlap, which further hindered the backbone assignment, resulting in the assignment of only 16 of 35 residues. 1D $^{1}H$ spectra of $^{13}C/^{15}N$-[S0,D8N]Pn3a at low pH revealed a fingerprint region that resembled a misfolded or disordered peptide (Figure 3D). 2D $^{1}H-^{15}N$ HSQC and 3D $^{1}H-^{15}N-^{13}C$ CBCA(CO)NH, HNCACB, and HBHA(CO)NH spectra of $^{13}C/^{15}N$-[S0,D8N]Pn3a acquired at pH 1.28 enabled the assignment of 31 out of 35 residues of conformer 1, while the spectra acquired at pH 3.45 enabled the assignment of the entirety of the backbone of conformer 2 (Figure 4A).

The comparison of the backbone chemical shifts of the earlier- and later-eluting peaks of the ligated peptide [D8N]-Pn3a-KIIIA corresponded well with the chemical shifts of unligated [D8N]Pn3a at pH 1.28 and 3.45, suggesting that the two conformations of the ligated peptide correspond to the same two conformations that arise from the modulation of pH (Figure 4A). Chemical shifts of conformer 2 were in close agreement with published Pn3a shifts, corresponding to a well-structured, typical ICK (Figures 4A and S5).[9] In contrast, many of the chemical shifts of conformer 1 were in poor agreement with the published Pn3a shifts and showed less deviation than conformer 2 from expected random coil chemical shift values reported in the Biological Magnetic Resonance Bank (Figures 4A and S5). This and the broad, less dispersed peaks observed in all NMR spectra suggest that conformer 1 adopts a secondary structure that more closely resembles a random coil than a rigidly structured ICK peptide, although the extent of the disorder is limited by the disulfide bonds maintained in the ICK scaffold.

Striking differences are easily observed between conformers 1 and 2 across all NMR spectra. 1D $^{1}H$ spectra of conformer 1 lacked several peaks, which gradually appeared as the peptide transitioned toward conformer 2 (Figure 3D), with amide proton peak dispersion ranging from 7.6−8.8 ppm for conformer 1 and 6.6−9.5 ppm for conformer 2. More than half of the C$\alpha$ chemical shifts of conformer 1 differed by more than 1 ppm from conformer 2 (Figure 4B,C).[9] The magnitudes of the C$\alpha$ chemical shift differences between conformers 1 and 2 were heat mapped on the structure of Pn3a (PDB 5T4R) (Figure 4C). N- and C-terminal residues generally had smaller ($\Delta\delta$ < 1 ppm) differences since they are outside of the ICK scaffold, particularly the C-terminal tail, which was flexible in solution in both conformations (Figure 4A,B).

Met5 and Phe6, which interact on the hydrophobic patch of conformer 2, showed C$\alpha$ shift differences greater than 2 ppm. Considerable chemical shift changes were also observed at Tyr27, which contributes to the hydrophobic patch and interacts with Met5 and Phe6. In conformer 2 spectra, the Tyr27 H$\alpha$ peak was found far downfield at 5.6 ppm, while the same peak was found in the average range, 1 ppm upfield, for conformer 1. Similarly, the Tyr27 C$\alpha$ peak had a chemical shift difference of nearly 2 ppm between the two conformers (Figure 4B,C). The Leu19 side-chain H$\delta$ shifts of conformer 2 were further upfield than average, appearing at 0.5 and 0.1 ppm due to interactions with other residues on the hydrophobic patch. For conformer 1, these shifts appeared at $\delta$ > 0.6 ppm (Figure 3D).

On the charged patch of the peptide, residues Lys11, Glu13, and Asp14 had 2−3 ppm C$\alpha$ shift differences between conformers (Figure 4B,C). These residues form salt bridges with one another, based on the published structure of Pn3a (PDB 5T4R) (Figure 4D).[9] Residues 15−19 produced peaks of very poor intensity that made unambiguous assignment impossible for conformer 1 and were flanked by residues that showed $\Delta\delta$ > 2. This suggests that loop 3 and the two cysteine residues preceding it are highly dynamic in the inactive conformer. Residues Asp12 and Arg23 showed the largest C$\alpha$ shift differences of 5.9 and 3.3 ppm, respectively (Figure 4B,C). These residues form a salt-bridge connecting loops 2 and 4 in conformer 2 (Figure 4D).[9]

## DISCUSSION AND CONCLUSIONS

The present study suggests that the conformational exchange that has long been observed chromatographically in some spider venom-derived peptides may be due to the acidic pH of HPLC solvents (~6.5 mM TFA, pH ~ 2.5). For Pn3a, the conformer (conformer 2) that dominates at higher pH is the conformer present in NMR and activity experiments, which are typically performed at pH ~ 4 and pH 7.4, respectively. A higher proportion of conformer 1 is present after incubation in 30% HPLC solvent B compared to HPLC solvent A. This may be due to differences in pH between the two solvents, or the formation of the inactive conformer may be assisted by the presence of an organic solvent. However, the organic solvent is not sufficient to cause conformational exchange without acidic pH. The data suggest that the published solution NMR structure for Pn3a corresponds to the later-eluting active conformation,[9] conformer 2, and the NMR structures that have been published for other peptides examined in this study, which were acquired at pH ~ 4, are likely capturing the active conformation.[31,38] This also suggests that only the active conformer 2 is present under normal physiological conditions. pH-dependent exchange may also have additional implications for these peptides in some potential applications, for example, formulation or dosage forms designed for oral administration. The drastic differences in the chemical shift between conformers 1 and 2 suggest that conformer 1 is largely unfolded, lacking many of the structural features found in the active conformer, and may be completely inactive. The apparent activity of conformer 1 of Pn3a-KIIIA[Srt] may be due to low-level contamination with conformer 2, which is inevitable due to the acidic RP-HPLC conditions used for purification.

Residues that form salt bridges tended to have larger chemical shift differences between the active and inactive conformers of Pn3a. Because conformer 1 dominates at low pH, this suggests that protonation of acidic residues may disrupt salt bridges, triggering a global change in the secondary structure. In the active conformer 2 structure of Pn3a, Asp12


https://doi.org/10.1021/acsomega.3c02664
ACS Omega 2023, 8, 26276−26286

and Arg23 form a salt bridge between loops 2 and 4. Glu13 and Asp14 form salt bridges with Lys11 within loop 2, which, along with backbone hydrogen bonding, stabilize an $\alpha$-helix directing Asp12 toward Arg23. The structural importance of Asp12, Asp14, and Tyr27 is further supported by a previous study in which the authors were unable to produce D12T, D14K, and Y27A mutants of Pn3a displaying native Pn3a disulfide connectivity and where the analogues were subsequently inactive.[10] On the other hand, E13K and E13A mutants in the same study were active and folded correctly, suggesting that salt bridges involving the side chain of this residue are not crucial for the structure of Pn3a. The loss of stabilizing salt bridges may cause loops 2 and 4 to become more disordered, resulting in broadened or missing NMR resonances for nearby residues. Disulfide bond rotational isomerization is also possible at Cys9, which has a 7.2 ppm C$\beta$ chemical shift difference between the two conformers, compared to 0.1−1.2 ppm differences at the other three assigned cysteine residues (Figure S5B). C$\beta$ resonances were not visible for Cys15 and Cys16. Tyr27 is involved in a $\pi-\pi$ interaction with Phe6, which connects loops 1 and 4 in the active conformer. This interaction may be lost in the inactive conformer, as evidenced by the lack of the deshielded Tyr27 H$\alpha$ proton at low pH (Figure 3D). Similarly, there is a CH/$\pi$ interaction between Leu19 and Trp30 in the active conformation, evidenced by the shielded Leu19 H$\delta$ protons. The loss of the shielding effect on the Leu19 side-chain protons in conformer 1 suggests that its position relative to Trp30 changes compared to conformer 2 (Figure 3D). The presence of the organic solvent may assist in disrupting hydrophobic interactions, favouring the inactive conformer.

Although the HPLC elution profile of Pn3a can strongly favor either conformer depending on the pH of the solvent used for peptide dissolution, many other spider venom peptides that exhibit conformational heterogeneity have a clear major and minor peak, even at pH 1. It is not clear why Pn3a is more sensitive to changes in pH than other peptides. Pn3a contains many acidic residues, particularly in loop 2 (Figure 1B), which may form salt bridges at neutral pH.[9] However, many of the acidic residues of Pn3a are not crucial for activity and correct folding, including Glu10 and Glu13 in loop 2.[10] The solution NMR structures of Pn3a, Hm1a, HaTx1, and SGTx1 show that all three peptides are stabilized in loop 2 by hydrogen bonding involving backbone amide protons, with Pn3a also forming salt bridges within loop 2.[9,31,38,39] In place of the salt-bridge forming Asp12 of Pn3a, Hm1a and HaTx1 contain a threonine residue that is involved in hydrogen bonding with the backbone of loop 4. This interaction would not be susceptible to protonation, making the active conformers of Hm1a and HaTx1 more stable at low pH. Similarly, SGTx1 contains a threonine at position 12, although this residue has not been shown to participate in hydrogen bonding with loop 4.

It is unclear why the exchange between conformer 1 and conformer 2 occurs more slowly when Pn3a is KIIIA-ligated to the N-terminus versus free or C-terminally ligated Pn3a. The key salt bridges are found nearer to the N-terminus of the peptide, which may explain why the extension of the C-terminus does not drastically affect the rate of exchange. An N-terminally biotinylated analogue of Pn3a, which removes the positive N-terminal charge, undergoes rapid exchange similarly to analogues with a charged N-terminus (Figure S6). The slowed rate of exchange is also unlikely to be due to specific interactions between Pn3a and KIIIA, as the same observation has been made for Pn3a containing other N-terminal extensions (Figure S7). Additionally, the 2D NMR spectra of both conformers of Pn3a-KIIIA produce nearly identical KIIIA peaks, suggesting a lack of stable interactions between the two segments (Figure S4). There may be interactions between the electrostatic face of Pn3a and the flexible polyglycine spacer between the two toxins, which influence the solvent exposure of the key aspartate residues and their rate of proton exchange, but this should give rise to chemical shift changes observable by NMR.

The rapid restoration of the structure as the monovalent peptide is moved from acidic to more neutral pH may be due to the ICK maintaining the residues in favorable positions to reform the correct salt bridges and other interactions. This suggests that this pH-dependence could potentially be exploited in the design of peptides as a "molecular switch" for use in the gastrointestinal tract,[40,41] lysosomes,[42] secretory granules,[43] and pH-altering states such as cancer,[44−47] inflammation,[48,49] ischemia,[50] and others.[51] Peptides containing acidic residues that are protonated in acidic environments to promote membrane insertion have been studied for cancer and inflammation,[45−47,49] and other pH-sensitive peptides have been studied for various applications.[52−61]

The present study characterizes the pH-dependent conformational exchange of Pn3a, suggesting that the protonation of acidic residues at low pH and the resulting charge neutralization disrupts crucial salt bridges. This causes a loss in overall structural integrity and activity in a peptide that contains an ICK, which is generally known to be stable at low pH. The peptide's intricate structure is easily restored by an increase in pH since the intact disulfide bonds keep the residues poised to reform their interactions. A similar phenomenon is observed for other spider venom-derived peptides with high sequence similarity to Pn3a. This is a novel explanation for the conformational heterogeneity of an ICK peptide where proline *cis*/*trans* isomerization and isoaspartate formation are not possible.

## EXPERIMENTAL SECTION

**Linear Peptide Assembly and Cleavage.** Pn3a and KIIIA analogues were assembled via Fmoc solid phase peptide synthesis on an automated microwave Liberty Prime synthesizer (CEM). Preloaded Wang polystyrene (LL) resins (CEM) were used at a 0.1 mmol scale for all Pn3a analogues and inactive N-terminal ligation KIIIA analogues, and Rink Amide resin (RAPP Polymere, Germany) was used for active C-terminal ligation KIIIA analogues. Coupling was performed with 0.5 M N-terminal Fmoc-protected and side-chain-protected amino acid/0.25 M Oxyma Pure/2 M *N*,*N*′-diisopropylcarbodiimide in *N*,*N*-dimethylformamide (DMF) (1 min at 105 °C). Fmoc deprotection was performed with 25% pyrrolidine/DMF (40 s at 100 °C).

Peptides were functionalized for N- to N-terminal copper-mediated azide-alkyne cycloaddition (CuAAC) ligation by manual coupling of Fmoc-L-propargylglycine to KIIIA analogues containing a polyglycine spacer, and Fmoc-N$^{\varepsilon}$-azide-L-lysine to Pn3a analogues. Manual coupling was performed using 4 eq amino acid/4 eq *O*-(1*H*-6-chlorobenzotriazole-1-yl)-1,1,3,3-tetramethyluronium hexafluorophosphate (HCTU)/6 eq *N*,*N*-diisopropylethylamine in DMF (5 min at room temperature). Fmoc deprotection was performed using 30% piperidine/DMF (10 min at room temperature).


https://doi.org/10.1021/acsomega.3c02664
ACS Omega 2023, 8, 26276−26286

Peptides were functionalized for C- to N-terminal enzymatic sortase A ligation by the inclusion of a polyglycine spacer at the N-terminus of KIIIA and the *Staphylococcus aureus* sortase A recognition motif LPATGG at the C-terminus of Pn3a.

Cleavage from resin and side-chain deprotection was performed simultaneously in 92.5% trifluoroacetic acid (TFA)/2.5% triisopropylsilane/2.5% 2,2-(ethylenedioxy)-diethanethiol/2.5% $H_2O$ (2 h at room temperature). Cleavage solutions were filtered to remove resin, and TFA was evaporated under $N_2$ flow. Peptides were precipitated, washed with cold diethyl ether, and centrifuged (3 × 5 min at 5000*g*). The final pellet was dissolved in 0.05% TFA/45% acetonitrile (ACN)/$H_2O$ and lyophilized. All peptides were confirmed to be >95% pure by HPLC analysis.

**Peptide Oxidation and Ligation.** KIIIA analogues were oxidized at 0.1 mg/mL in 0.1 M $NH_4HCO_3$ at pH 8 (24 h at room temperature). Pn3a analogues were oxidized at 0.1 mg/mL in 4.5 M $NH_4OAc$ at pH 8 with 2 M urea and 1:10 oxidized to reduced glutathione (48 h at 4 °C). Oxidation solutions were acidified to pH < 4 with TFA, filtered, and purified by RP-HPLC. Correct peptide folding was confirmed by ESI-MS and 1D and 2D $^1H$ NMR.

N- to N-terminal CuAAC ligation was performed with 1:2 azide- and alkyne-containing peptides in 50 mM potassium phosphate buffer at pH 7 treated with premixed copper(II) sulfate and tris-hydroxypropyltriazolylmethylamine (for final concentrations of 0.1 and 0.5 mM, respectively), 5 mM aminoguanidine, and 5 mM sodium ascorbate under a $N_2$ atmosphere (2 h at 37 °C). Reactions were quenched by cooling and acidification with 1% TFA/$H_2O$ to pH < 4, then filtered and purified by RP-HPLC. Successful ligation was confirmed by ESI-MS and 1D and 2D NMR.

C- to N-terminal sortase A ligation was performed by dissolving sortase-functionalized peptides in 50 mM Tris buffer at pH 8 containing 150 mM NaCl and 10 mM $CaCl_2$, followed by treatment with the *S. aureus* sortase A pentamutant SrtA5 at a ratio of 1:3:6 SrtA5:Pn3a:KIIIA (15 min at 37 °C). Reactions were quenched by cooling and acidification with 1% TFA/$H_2O$ to pH < 4 and then filtered and purified by RP-HPLC. The successful ligation product was confirmed by ESI-MS.

**RP-HPLC and Mass Spectrometry.** A Shimadzu LC-20AP (Shimadzu, Japan) solvent delivery module equipped with an SPD-20A (Shimadzu) UV/vis detector was used for preparative HPLC. Preparative HPLC was performed using a Luna C8 column (Phenomenex; 15 μm, 250 mm × 50 mm, 100 Å, 50 mL/min) or a Zorbax 300SB C18 column (Agilent; 5 μm, 21.2 mm × 150 mm, 300 Å, 20 mL/min). Semi-preparative HPLC was performed using a Zorbax 300SB C8 column (Agilent; 5 μm, 9.4 mm × 150 mm, 300 Å, 3 mL/min). A Shimadzu LC-40D XR (Shimadzu) solvent delivery module equipped with an SPD-40V (Shimadzu) UV/vis detector and SIL-40 XR (Shimadzu) autosampler was used for analytical HPLC. Analytical HPLC was performed using a Zorbax 300SB C18 column (Agilent; 5 μm, 4.6 mm × 250 mm, 300 Å, 1 mL/min) or a Hypersil GOLD C18 column (Thermo Fisher Scientific; 3 μm, 2.1 mm × 100 mm, 175 Å, 0.6 mL/min). Gradients were run from solvent A (0.05% TFA/$H_2O$) to solvent B (0.05% TFA/90% ACN/$H_2O$), and absorbance was monitored at 214 and 280 nm. Peptide masses were confirmed by electrospray ionization mass spectrometry (ESI-MS) on an API 2000 LC/MS/MS system (AB SCIEX) or time-of-flight (TOF) LC/MS on a TripleTOF 5600 system (AB SCIEX) equipped with an LC-30AD (Shimadzu) solvent delivery module, a SIL-30AC (Shimadzu) autosampler, and a CTO-20A (Shimadzu) column oven.

**Automated Whole-Cell Patch-Clamp Electrophysiology.** HEK 293 cells stably expressing human $Na_V1.7$ and $\beta1$ subunits (SB Drug Discovery, U.K.) were cultured in minimum essential medium (MEM) supplemented with 10% (v/v) heat-inactivated fetal bovine serum, 1% (v/v) GlutaMAX, 4 μg/mL blasticidin, and 0.6 mg/mL geneticin. Cells were passaged at 70−80% confluence using TrypLE Express for dissociation.

Automated whole-cell patch-clamp electrophysiology assays were performed on a QPatch II platform (Sophion Bioscience, Denmark) as previously described (PMID: **33023152**). Cells were dissociated and gently stirred in serum-free MEM containing 25 mM HEPES, 100 U/mL penicillin-streptomycin, and 0.04 mg/mL soybean trypsin inhibitor for 30−60 min before use. The extracellular solution (ECS) comprised 70 mM NaCl, 70 mM choline chloride, 4 mM KCl, 2 mM $CaCl_2$, 1 mM $MgCl_2$, 10 mM HEPES, and 10 mM glucose, adjusted to pH 7.4 and 305 mOsm. The intracellular solution comprised 140 mM CsF, 1 mM EGTA, 5 mM CsOH, 10 mM HEPES, and 10 mM NaCl, adjusted to pH 7.3 (using CsOH) and 320 mOsm. Peptides were diluted in ECS containing 0.1% bovine serum albumin.

Concentration−response curves were acquired at a holding potential of −90 mV with a 50 ms pulse to −20 mV every 20 s. Peptide concentrations were incubated for 5 min each, and peak currents were normalized to buffer controls. GraphPad Prism 9.3.1 was used to fit a four-parameter Hill equation with a variable Hill coefficient.

**DNA Mutagenesis and Bacterial Expression.** $^{13}C/^{15}N$-labeled [S0,D8N]Pn3a was produced by recombinant expression in *Escherichia coli*. The WT Pn3a/pLIC vector with SUMO-tag cDNA was subjected to in vitro site-directed mutagenesis using the QuikChange Lightning mutagenesis kit (Agilent Technologies) following the manufacturer's instructions. The following point mutations were created in the WT Pn3a/pLIC vector with SUMO-tag cDNA: G0S and D8N, using the following two oligonucleotides: 5′- CAGAGTGATTGCCGTTATATGTTTGGCAATTGTG-3′ and 5′-CACAATTGCCAAACATATAACGGCAATCACTCTG-3′. Mutations were verified by sequencing by the Australian Genome Research Facility.

The vector was transformed into competent SHuffle cells (New England Biolabs) by heat shock, plated on ampicillin selection plates, and incubated at 30 °C overnight. A 10 mL Luria−Bertani (LB) media primary culture with ampicillin selection was inoculated with one colony and shaken at 30 °C overnight. Four 1 L LB media cultures with ampicillin selection were inoculated with the primary culture and shaken at 30 °C until the optical density at 600 nm ($OD_{600}$) reached ∼0.8. Cells were pelleted at 5000*g* and resuspended in M9 media containing 0.1% w/v $^{15}NH_4Cl$ and 0.4% w/v $^{13}C_6$-D-glucose and then incubated at 30 °C for 30 min. Cells were induced with 0.5 mM isopropyl β-D-1-thiogalactopyranoside (IPTG) and shaken at 30 °C for 5 h. Cells were pelleted at 5000*g* and resuspended in RS-1 lysis buffer (20 mM Tris at pH 7.8 with 500 mM NaCl) with 1 mg lysozyme and sonicated at 4 °C. Cell debris was pelleted at 40 000*g*, and the soluble protein extract was loaded onto a 5 mL HisTrap FF column (Cytiva) pre-equilibrated with lysis buffer. The column was washed with lysis buffer containing 25 mM imidazole, and SUMO-Pn3a was eluted from the column with lysis buffer containing 250 mM


https://doi.org/10.1021/acsomega.3c02664
ACS Omega 2023, 8, 26276−26286

imidazole. The eluted protein was buffer exchanged to 20 mM Tris pH 7.8 using an Amicon 10 kDa cutoff centrifugal concentrator (Merck). Pn3a was cleaved from SUMO with 1 mg $His_6$-tagged TEV protease in 20 mM Tris buffer at pH 7.8 containing 5 mM DTT at room temperature overnight. The cleaved protein solution was acidified with 0.5% TFA, filtered to remove precipitation, and purified using RP-HPLC on a Vydac C18 column (GRACE; 10 $\mu$m, 10 mm × 250 mm, 300 Å). Fractions containing linear Pn3a, determined using matrix-assisted laser desorption/ionization time-of-flight mass spectrometry, were pooled and lyophilized.

**NMR Spectroscopy.** Unlabeled peptides were dissolved at ~500 $\mu$M in 500 $\mu$L of 10% $D_2O/H_2O$ and pH was measured to confirm pH ~ 4. $^{13}C/^{15}N$-labeled Pn3a was dissolved at ~350 $\mu$M in 300 $\mu$L of 10% $D_2O/H_2O$ in a Shigemi tube. Spectra were acquired at 298 K on a Bruker Avance 900 MHz spectrometer (Bruker) equipped with a triple-resonance TCI cryoprobe (Bruker) and processed using TopSpin 4.1.3 (Bruker). NMR resonances of different conformers were assigned at pH 1.28 and 3.45, respectively, using a combination of 2D and 3D experiments: $^1H-^1H$ TOCSY (80 ms mixing time), $^1H-^1H$ NOESY (200 ms mixing time), $^1H-^{15}N$ HSQC, $^1H-^{13}C-^{15}N$ CBCACONH, and HNCACB NMR experiments. NMR data analysis and resonance assignments were carried out using CCPNMR Analysis (CCPN, U.K.). Additional 1D $^1H$ spectra and 2D $^1H-^{15}N$ HSQC were recorded as a function of pH to track conformational exchange. pH was adjusted incrementally with HCl or NaOH and measured by a pH meter after each pH change, and water referencing was adjusted after each pH change.

**RP-HPLC Conformational Exchange Assays.** For RP-HPLC exchange assays, peptides were dissolved in varying solvents at 5−10 $\mu$M and injected via an autosampler at specified time points. pH 1 was achieved at 100 mM HCl, pH 3 and 7 buffers were 20 mM potassium phosphate, and pH 5 buffer was 20 mM sodium citrate. All peptides were run on a 0−50% solvent B gradient over 12.5 min on an analytical HPLC column. The area under the curve (AUC) from the 214 nm trace was measured using manual integration in LabSolutions 5.97 (Shimadzu). Individual peaks were normalized to the total peptide AUC of each trace. Time constants ($\tau$) were calculated by fitting curves to a one-phase decay.

## ■ ASSOCIATED CONTENT

### Supporting Information

The Supporting Information is available free of charge at https://pubs.acs.org/doi/10.1021/acsomega.3c02664.

Table with sequences of peptides, total ion chromatograms, and masses from liquid chromatography/mass spectrometry, analytical RP-HPLC chromatograms and masses of peptides used in the study, 2D $^1H$ NMR spectra of [D8N]Pn3a conformer 1 and 2, secondary backbone NMR chemical shifts, and time-course study of XTEN-Pn3a at pH 1 (PDF)

## ■ AUTHOR INFORMATION


### Corresponding Authors

**Christina I. Schroeder** − *Institute for Molecular Bioscience, The University of Queensland, Brisbane, Queensland 4072, Australia; Center for Cancer Research, National Cancer Institute, National Institutes of Health, Frederick, Maryland 21702-1201, United States; Genentech, South San Francisco, California 94080, United States;* orcid.org/0000-0002-6737-6374; Email: schroeder.christina@gene.com

**Irina Vetter** − *Institute for Molecular Bioscience, The University of Queensland, Brisbane, Queensland 4072, Australia; School of Pharmacy, The University of Queensland, Brisbane, Queensland 4102, Australia;* orcid.org/0000-0002-3594-9588; Email: i.vetter@imb.uq.edu.au

### Authors

**Poanna Tran** − *Institute for Molecular Bioscience, The University of Queensland, Brisbane, Queensland 4072, Australia;* orcid.org/0000-0003-3196-9896

**Theo Crawford** − *Centre for Advanced Imaging, The University of Queensland, Brisbane, Queensland 4072, Australia;* orcid.org/0000-0002-1101-5705

**Lotten Ragnarsson** − *Institute for Molecular Bioscience, The University of Queensland, Brisbane, Queensland 4072, Australia*

**Jennifer R. Deuis** − *Institute for Molecular Bioscience, The University of Queensland, Brisbane, Queensland 4072, Australia*

**Mehdi Mobli** − *Centre for Advanced Imaging, The University of Queensland, Brisbane, Queensland 4072, Australia*

**Simon J. Sharpe** − *Molecular Medicine Program, Research Institute, The Hospital for Sick Children, Toronto, Ontario M5G 0A4, Canada; Department of Biochemistry, University of Toronto, Toronto, Ontario M5S 1A8, Canada*

Complete contact information is available at: https://pubs.acs.org/10.1021/acsomega.3c02664



### Funding

This work was funded by the Australian National Health and Medical Research Council (NMHRC) through an Ideas Grant (2002860) awarded to C.I.S./I.V. I.V. is supported by an NHMRC Career Development Fellowship (APP1162503). J.R.D. is supported by an Australian Research Council (ARC) DECRA Fellowship (DE210100422). C.I.S. was supported by an ARC Future Fellowship (FT160100055) during part of the study. P.T. is supported by a University of Queensland Research Training Scholarship. This work was also supported [in part] by the Intramural Research Program of the National Cancer Institute, Center for Cancer Research (Grant ZIA BC 012003).


### Notes

The authors declare the following competing financial interest(s): C.I.S. is an employee of Genentech, Inc. and shareholder of Roche.

## ■ ACKNOWLEDGMENTS


The authors would like to thank Alexander Mueller, Hue N.T. Tran, Zoltan Dekan, Chun Yuen Chow, the SPARC lab, the Houry lab, and the Deber lab. The authors would also like to acknowledge Prof. David Liu, Harvard University, for his kind gift of the SrtA pentamutant plasmid.


## ■ REFERENCES


(1) Catterall, W. A.; Cestele, S.; Yarov-Yarovoy, V.; Yu, F. H.; Konoki, K.; Scheuer, T. Voltage-gated ion channels and gating modifier toxins. *Toxicon* **2007**, *49*, 124−141.

(2) Pennington, M. W.; Czerwinski, A.; Norton, R. S. Peptide therapeutics from venom: current status and potential. *Bioorg. Med. Chem.* **2018**, *26*, 2738−2758.
(3) Maatuf, Y.; Geron, M.; Priel, A. The role of toxins in the pursuit for novel analgesics. *Toxins* **2019**, *11*, No. 131.
(4) Vetter, I.; Deuis, J. R.; Mueller, A.; Israel, M. R.; Starobova, H.; Zhang, A.; Rash, L. D.; Mobli, M. $Na_V1.7$ as a pain target − from gene to pharmacology. *Pharmacol. Ther.* **2017**, *172*, 73−100.
(5) Catterall, W. A. From ionic currents to molecular mechanisms: the structure and function of voltage-gated sodium channels. *Neuron* **2000**, *26*, 13−25.
(6) Cox, J. J.; Reimann, F.; Nicholas, A. K.; Thornton, G.; Roberts, E.; Springell, K.; Karbani, G.; Jafri, H.; Mannan, J.; Raashid, Y.; Al-Gazali, L.; Hamamy, H.; Valente, E. M.; Gorman, S.; Williams, R.; McHale, D. P.; Wood, J. N.; Gribble, F. M.; Woods, C. G. An *SCN9A* channelopathy causes congenital inability to experience pain. *Nature* **2006**, *444*, 894−898.
(7) Dib-Hajj, S. D.; Rush, A. M.; Cummins, T. R.; Hisama, F. M.; Novella, S.; Tyrrell, L.; Marshall, L.; Waxman, S. G. Gain-of-function mutation in $Na_V1.7$ in familial erythromelalgia induces bursting of sensory neurons. *Brain* **2005**, *128*, 1847−1854.
(8) Fischer, T. Z.; Gilmore, E. S.; Estacion, M.; Eastman, E.; Taylor, S.; Melanson, M.; Dib-Hajj, S. D.; Waxman, S. G. A novel $Na_V1.7$ mutation producing carbamazepine-responsive erythromelalgia. *Ann. Neurol.* **2009**, *65*, 733−741.
(9) Deuis, J. R.; Dekan, Z.; Wingerd, J. S.; Smith, J. J.; Munasinghe, N. R.; Bhola, R. F.; Imlach, W. L.; Herzig, V.; Armstrong, D. A.; Rosengren, K. J.; Bosmans, F.; Waxman, S. G.; Dib-Hajj, S. D.; Escoubas, P.; Minett, M. S.; Christie, M. J.; King, G. F.; Alewood, P. F.; Lewis, R. J.; Wood, J. N.; Vetter, I. Pharmacological characterisation of the highly $Na_V1.7$ selective spider venom peptide Pn3a. *Sci. Rep.* **2017**, *7*, No. 40883.
(10) Mueller, A.; Dekan, Z.; Kaas, Q.; Agwa, A. J.; Starobova, H.; Alewood, P. F.; Schroeder, C. I.; Mobli, M.; Deuis, J. R.; Vetter, I. Mapping the molecular surface of the analgesic $Na_V1.7$-selective peptide Pn3a reveals residues essential for membrane and channel interactions. *ACS Pharmacol. Transl. Sci.* **2020**, *3*, 535−546.
(11) Agwa, A. J.; Huang, Y. H.; Craik, D. J.; Henriques, S. T.; Schroeder, C. I. Lengths of the C-terminus and interconnecting loops impact stability of spider-derived gating modifier toxins. *Toxins* **2017**, *9*, 248−262.
(12) Herzig, V.; King, G. F. The cystine knot is responsible for the exceptional stability of the insecticidal spider toxin $\omega$-hexatoxin-Hv1a. *Toxins* **2015**, *7*, 4366−4380.
(13) Sharma, G.; Deuis, J. R.; Jia, X.; Mueller, A.; Vetter, I.; Mobli, M. Recombinant production, bioconjugation and membrane binding studies of Pn3a, a selective $Na_V1.7$ inhibitor. *Biochem. Pharmacol.* **2020**, *181*, No. 114148.
(14) Cardoso, F. C.; Dekan, Z.; Smith, J. J.; Deuis, J. R.; Vetter, I.; Herzig, V.; Alewood, P. F.; King, G. F.; Lewis, R. J. Modulatory features of the novel spider toxin $\mu$-TRTX-Df1a isolated from the venom of the spider *Davus fasciatus*. *Br. J. Pharmacol.* **2017**, *174*, 2528−2544.
(15) Klint, J. K.; Berecki, G.; Durek, T.; Mobli, M.; Knapp, O.; King, G. F.; Adams, D. J.; Alewood, P. F.; Rash, L. D. Isolation, synthesis and characterization of $\omega$-TRTX-Cc1a, a novel tarantula venom peptide that selectively targets L-type $Ca_V$ channels. *Biochem. Pharmacol.* **2014**, *89*, 276−286.
(16) Swartz, K. J.; MacKinnon, R. Mapping the receptor site for hanatoxin, a gating modifier of voltage-dependent $K^+$ channels. *Neuron* **1997**, *18*, 675−682.
(17) Omecinsky, D. O.; Holub, K. E.; Adams, M. E.; Reily, M. D. Three-dimensional structure analysis of $\mu$-agatoxins: further evidence for common motifs among neurotoxins with diverse ion channel specificities. *Biochemistry* **1995**, *35*, 2836−2844.
(18) Rosengren, K. J.; Wilson, D.; Daly, N. L.; Alewood, P. F.; Craik, D. J. Solution structures of the *cis*- and *trans*-Pro30 isomers of a novel 38-residue toxin from the venom of *Hadronyche infensa sp*. that contains a cystine-knot motif within its four disulfide bonds. *Biochemistry* **2002**, *41*, 3294−3301.
(19) Jin, A. H.; Brandstaetter, H.; Nevin, S. T.; Tan, C. C.; Clark, R. J.; Adams, D. J.; Alewood, P. F.; Craik, D. J.; Daly, N. L. Structure of $\alpha$-conotoxin BuIA: influences of disulfide connectivity on structural dynamics. *BMC Struct. Biol.* **2007**, *7*, No. 28.
(20) Andreotti, A. H. Native state proline isomerization: an intrinsic molecular switch. *Biochemistry* **2003**, *42*, 9515−9524.
(21) Guttman, M.; Padte, N. N.; Huang, Y.; Yu, J.; Rocklin, G. J.; Weitzner, B. D.; Scian, M.; Ho, D. D.; Lee, K. K. The influence of proline isomerization on potency and stability of anti-HIV antibody 10E8. *Sci. Rep.* **2020**, *10*, No. 14313.
(22) Joseph, A. P.; Srinivasan, N.; de Brevern, A. G. *Cis-trans* peptide variations in structurally similar proteins. *Amino Acids* **2012**, *43*, 1369−1381.
(23) Lummis, S. C. R.; Beene, D. L.; Lee, L. W.; Lester, H. A.; Broadhurst, R. W.; Dougherty, D. A. *Cis-trans* isomerization at a proline opens the pore of a neurotransmitter-gated ion channel. *Nature* **2005**, *438*, 248−252.
(24) Taler-Verčič, A.; Hasanbasic, S.; Berbic, S.; Stoka, V.; Turk, D.; Zerovnik, E. Proline residues as switches in conformational changes leading to amyloid fibril formation. *Int. J. Mol. Sci.* **2017**, *18*, No. 549.
(25) Bae, C.; Kalia, J.; Song, I.; Yu, J.; Kim, H. H.; Swartz, K. J.; Kim, J. I. High yield production and refolding of the double-knot toxin, an activator of TRPV1 channels. *PLoS One* **2012**, *7*, No. e51516.
(26) Smith, J. J.; Herzig, V.; Ikonomopoulou, M. P.; Dziemborowicz, S.; Bosmans, F.; Nicholson, G. M.; King, G. F. Insect-active toxins with promiscuous pharmacology from the African theraphosid spider *Monocentropus balfouri*. *Toxins* **2017**, *9*, No. 155.
(27) Johnson, S. R.; Rikli, H. G. Aspartic acid isomerization characterized by high definition mass spectrometry significantly alters the bioactivity of a novel toxin from *Poecilotheria*. *Toxins* **2020**, *12*, No. 207.
(28) Swartz, K. J.; MacKinnon, R. An inhibitor of the $K_V2.1$ potassium channel isolated from the venom of a Chilean tarantula. *Neuron* **1995**, *15*, 941−949.
(29) Deuis, J. R.; Ragnarsson, L.; Robinson, S. D.; Dekan, Z.; Chan, L.; Jin, A. H.; Tran, P.; McMahon, K. L.; Li, S.; Wood, J. N.; Cox, J. J.; King, G. F.; Herzig, V.; Vetter, I. The tarantula venom peptide Eo1a binds to the domain II S3-S4 extracellular loop of voltage-gated sodium channel $Na_V1.8$ to enhance activation. *Front. Pharmacol.* **2021**, *12*, No. 789570.
(30) Osteen, J. D.; Herzig, V.; Gilchrist, J.; Emrick, J. J.; Zhang, C.; Wang, X.; Castro, J.; Garcia-Caraballo, S.; Grundy, L.; Rychkov, G. Y.; Weyer, A. D.; Dekan, Z.; Undheim, E. A. B.; Alewood, P.; Stucky, C. L.; Brierley, S. M.; Basbaum, A. I.; Bosmans, F.; King, G. F.; Julius, D. Selective spider toxins reveal a role for the $Na_V1.1$ channel in mechanical pain. *Nature* **2016**, *534*, 494−499.
(31) Takahashi, H.; Kim, J. I.; Min, H. J.; Sato, K.; Swartz, K. J.; Shimada, I. Solution structure of hanatoxin1, a gating modifier of voltage-dependent $K^+$ channels: common surface features of gating modifier toxins. *J. Mol. Biol.* **2000**, *297*, 771−780.
(32) Otting, G.; Liepinsh, E.; Wüthrich, K. Disulfide bond isomerization in BPTI and BPTI(G36S): an NMR study of correlated mobility in proteins. *Biochemistry* **1993**, *32*, 3571−3582.
(33) Wagner, G.; DeMarco, A.; Wüthrich, K. Dynamics of the aromatic amino acid residues in the globular conformation of the basic pancreatic trypsin inhibitor (BPTI) I. $^1H$ NMR studies. *Biophys. Struct. Mech.* **1976**, *2*, 139−158.
(34) Wingerd, J. S.; Mozar, C. A.; Ussing, C. A.; Murali, S. S.; Chin, Y. K.; Cristofori-Armstrong, B.; Durek, T.; Gilchrist, J.; Vaughan, C. W.; Bosmans, F.; Adams, D. J.; Lewis, R. J.; Alewood, P. F.; Mobli, M.; Christie, M. J.; Rash, L. D. The tarantula toxin $\beta/\delta$-TRTX-Pre1a highlights the importance of the S1-S2 voltage-sensor region for sodium channel subtype selectivity. *Sci. Rep.* **2017**, *7*, No. 974.
(35) Tran, H. N. T.; Tran, P.; Deuis, J. R.; Agwa, A. J.; Zhang, A. H.; Vetter, I.; Schroeder, C. I. Enzymatic ligation of a pore blocker toxin and a gating modifier toxin: creating double-knotted peptides with


https://doi.org/10.1021/acsomega.3c02664
*ACS Omega* 2023, 8, 26276−26286

improved sodium channel $Na_V1.7$ inhibition. *Bioconjugate Chem.* **2020**, *31*, 64−73.
(36) Marvin, L.; De, E.; Cosette, P.; Gagnon, J.; Molle, G.; Lange, C. Isolation, amino acid sequence and functional assays of SGTx1. *Eur. J. Biochem.* **1999**, *265*, 572−579.
(37) Middleton, R. E.; Warren, V. A.; Kraus, R. L.; Hwang, J. C.; Liu, C. J.; Dai, G.; Brochu, R. M.; Kohler, M. G.; Gao, Y.-D.; Garsky, V. M.; Bogusky, M. J.; Mehl, J. T.; Cohen, C. J.; Smith, M. M. Two tarantula peptides inhibit activation of multiple sodium channels. *Biochemistry* **2002**, *41*, 14734−14747.
(38) Richards, K. L.; Milligan, C. J.; Richardson, R. J.; Jancovski, N.; Grunnet, M.; Jacobsen, L. H.; Undheim, E. A. B.; Mobli, M.; Chow, C. Y.; Herzig, V.; Costi, A.; Panyi, G.; Reid, C. A.; King, G. F.; Petrou, S. A selective $Na_V1.1$ activator rescues Dravet syndrome mice from seizures and premature death. *Proc. Natl. Acad. Sci. U.S.A.* **2018**, *115*, E8077−E8085.
(39) Lee, C. W.; Kim, S.; Roh, S. H.; Endoh, H.; Kodera, H.; Maeda, T.; Kohno, T.; Wang, J. M.; Swartz, K. J.; Kim, J. I. Solution structure and functional characterization of SGTx1, a modifier of $K_V2.1$ channel gating. *Biochemistry* **2004**, *43*, 890−897.
(40) Evans, D. F.; Pye, G.; Bramley, R.; Clark, A. G.; Dyson, T. J.; Hardcastle, J. D. Measurement of gastrointestinal pH profiles in normal ambulant human subjects. *Gut* **1988**, *29*, 1035−1041.
(41) Cardoso, F. C.; Castro, J.; Grundy, L.; Schober, G.; Garcia-Caraballo, S.; Zhao, T.; Herzig, V.; King, G. F.; Brierley, S. M.; Lewis, R. J. A spider-venom peptide with multitarget activity on sodium and calcium channels alleviates chronic visceral pain in a model of irritable bowel syndrome. *Pain* **2021**, *162*, 569−581.
(42) Chen, R.; Jaattela, M.; Liu, B. Lysosome as a central hub for rewiring pH homeostasis in tumors. *Cancers* **2020**, *12*, No. 2437.
(43) Urbé, S.; Dittié, A. S.; Tooze, S. A. pH-dependent processing of secretogranin II by the endopeptidase PC2 in isolated immature secretory granules. *Biochem. J.* **1997**, *321*, 65−74.
(44) Justus, C. R.; Dong, L.; Yang, L. V. Acidic tumor microenvironment and pH-sensing G protein-coupled receptors. *Front. Physiol.* **2013**, *4*, No. 354.
(45) Andreev, O. A.; Dupuy, A. D.; Segala, M.; Sandugu, S.; Serra, D. A.; Chichester, C. O.; Engelman, D. M.; Reshetnyak, Y. K. Mechanism and uses of a membrane peptide that targets tumors and other acidic tissues in vivo. *Proc. Natl. Acad. Sci. U.S.A.* **2007**, *104*, 7893−7898.
(46) Wyatt, L. C.; Moshnikova, A.; Crawford, T.; Engelman, D. M.; Andreev, O. A.; Reshetnyak, Y. K. Peptides of pHLIP family for targeted intracellular and extracellular delivery of cargo molecules to tumors. *Proc. Natl. Acad. Sci. U.S.A.* **2018**, *115*, E2811−E2818.
(47) Weerakkody, D.; Moshnikova, A.; El-Sayed, N. S.; Adochite, R. C.; Slaybaugh, G.; Golijanin, J.; Tiwari, R. K.; Andreev, O. A.; Parang, K.; Reshetnyak, Y. K. Novel pH-sensitive cyclic peptides. *Sci. Rep.* **2016**, *6*, No. 31322.
(48) Rajamäki, K.; Nordstrom, T.; Nurmi, K.; Akerman, K. E.; Kovanen, P. T.; Oorni, K.; Eklund, K. K. Extracellular acidosis is a novel danger signal alerting innate immunity via the NLRP3 inflammasome. *J. Biol. Chem.* **2013**, *288*, 13410−13419.
(49) Visca, H.; DuPont, M.; Moshnikova, A.; Crawford, T.; Engelman, D. M.; Andreev, O. A.; Reshetnyak, Y. K. pHLIP peptides target acidity in activated macrophages. *Mol. Imaging Biol.* **2022**, *24*, 874−885.
(50) Chassagnon, I. R.; McCarthy, C. A.; Chin, Y. K.; Pineda, S. S.; Keramidas, A.; Mobli, M.; Pham, V.; De Silva, T. M.; Lynch, J. W.; Widdop, R. E.; Rash, L. D.; King, G. F. Potent neuroprotection after stroke afforded by a double-knot spider-venom peptide that inhibits acid-sensing ion channel 1a. *Proc. Natl. Acad. Sci. U.S.A.* **2017**, *114*, 3750−3755.
(51) Gebert, G.; Benzing, H.; Strohm, M. Changes in the interstitial pH of dog myocardium in response to local ischemia, hypoxia, hyper- and hypocapnia, measured continuously by means of glass micro-electrodes. *Pflügers Arch.* **1971**, *329*, 72−81.
(52) Schach, D. K.; Rock, W.; Franz, J.; Bonn, M.; Parekh, S. H.; Weidner, T. Reversible activation of a cell-penetrating peptide in a membrane environment. *J. Am. Chem. Soc.* **2015**, *137*, 12199−12202.
(53) Turk, M. J.; Reddy, J. A.; Chmielewski, J. A.; Low, P. S. Characterization of a novel pH-sensitive peptide that enhances drug release from folate-targeted liposomes at endosomal pHs. *Biochim. Biophys. Acta, Biomembr.* **2002**, *1559*, 56−68.
(54) Choi, H.; Cao, J.; Qiao, H.; Chen, I. W.; Zhou, R. Improving cancer detection and treatment by pH-sensitive peptide nanoparticle drug delivery platform: pharmacokinetics, toxicity, and immunogenicity profile. *Adv. Nanobiomed. Res.* **2022**, *2*, No. 2100081.
(55) Hitchner, M. A.; Santiago-Ortiz, L. E.; Necelis, M. R.; Shirley, D. J.; Palmer, T. J.; Tarnawsky, K. E.; Vaden, T. D.; Caputo, G. A. Activity and characterization of a pH-sensitive antimicrobial peptide. *Biochim. Biophys. Acta, Biomembr.* **2019**, *1861*, No. 182984.
(56) Ding, L.; Jiang, Y.; Zhang, J.; Klok, H. A.; Zhong, Z. pH-sensitive coiled-coil peptide-cross-linked hyaluronic acid nanogels: synthesis and targeted intracellular protein delivery to CD44 positive cancer cells. *Biomacromolecules* **2018**, *19*, 555−562.
(57) Escoubas, P.; Diochot, S.; Celerier, M.-L.; Nakajima, T.; Lazdunski, M. Novel tarantula toxins for subtypes of voltage-dependent potassium channels in the $K_V2$ and $K_V4$ subfamilies. *Mol. Pharmacol.* **2002**, *62*, 48−57.
(58) Siemens, J.; Zhou, S.; Piskorowski, R.; Nikai, T.; Lumpkin, E. A.; Basbaum, A. I.; King, D.; Julius, D. Spider toxins activate the capsaicin receptor to produce inflammatory pain. *Nature* **2006**, *444*, 208−212.
(59) Agwa, A. J.; Peigneur, S.; Chow, C. Y.; Lawrence, N.; Craik, D. J.; Tytgat, J.; King, G. F.; Henriques, S. T.; Schroeder, C. I. Gating modifier toxins isolated from spider venom: modulation of voltage-gated sodium channels and the role of lipid membranes. *J. Biol. Chem.* **2018**, *293*, 9041−9052.
(60) Rupasinghe, D. B.; Herzig, V.; Vetter, I.; Dekan, Z.; Gilchrist, J.; Bosmans, F.; Alewood, P. F.; Lewis, R. J.; King, G. F. Mutational analysis of ProTx-I and the novel venom peptide Pe1b provide insight into residues responsible for selective inhibition of the analgesic drug target $Na_V1.7$. *Biochem. Pharmacol.* **2020**, *181*, No. 114080.
(61) Wei, P.; Xu, C.; Wu, Q.; Huang, L.; Liang, S.; Yuan, C. Jingzhaotoxin-35, a novel gating-modifier toxin targeting both $Na_V1.5$ and $K_V2.1$ channels. *Toxicon* **2014**, *92*, 90−96.


https://doi.org/10.1021/acsomega.3c02664
*ACS Omega* 2023, 8, 26276−26286